Journal of Bio- and Tribo-Corrosion (2018) 4:8
https://doi.org/10.1007/s40735-017-0124-x

Prosopis juliflora Plant Extract as Potential Corrosion Inhibitor for Low-Carbon Steel in 1 M HCl Solution

A. S. Fouda[1] · G. Y. El-Awady[1] · W. T. El Behairy[1]

Received: 27 September 2017 / Revised: 26 November 2017 / Accepted: 6 December 2017 / Published online: 20 December 2017

Abstract
Herein, *Prosopis juliflora* (PJF) plant extract was assessed as a low-cost, green and efficient corrosion inhibitor for low-carbon steel (LCS) in 1 M hydrochloric acid solution using mass loss, gasometric, electrochemical impedance spectroscopy, potentiodynamic polarization, electrochemical frequency modulation methods as well as surface studies by scanning electronic microscope (SEM) and atomic force microscope (AFM). Increasing (PJF) extract concentration increases the charge transfer resistance (R_{ct}) and decreases the double-layer capacitance (C_{dl}) as a result of the adsorption of PJF extract on the LCS surface. The polarization results showed the mixed-type inhibition behavior of the studied extract with inhibition efficiency (%IE) of 90.7% achieved with the addition of 300 ppm of PJF. The adsorption isotherm model of PJF extract on LCS surface followed Temkin adsorption isotherm in HCl solution. The inhibition mechanism of PJF was explained according to the increase in the %IE with temperature and the activation parameters which suggested significant chemisorption of the PJF extract on the LCS surface. The AFM and SEM studies confirmed the formation of protective layer of PJF extract on LCS surface. Results obtained by different techniques showed good agreement which confirm the potential use of PJF extract as corrosion inhibitor for LCS in acidic media.

Keywords *Prosopis juliflora* extract · Corrosion inhibition · Low-carbon steel · HCl · SEM · AFM

1 Introduction

Hydrochloric acid (HCl) solutions are widely used for acid cleaning, industry acid pickling, oil well acidizing and acid descaling [1–4], but hydrochloric acid medium has aggressive effect on substances. Plant extracts are considered cheap, safety, on-hand and renewable sources of inhibitors. The plant extracts include different organic compounds containing heteroatoms, and some [5–8] have been to act as metal dissolution inhibitors in various corrosive mediums. "So, we need the using of substances that have inhibiting effect to protect the metals which used in different fields of applications. The formation of thin layer resulting from interaction of organic compounds on the metal (mixed inhibitors) while in case of inorganic inhibitors may block anodic or/and cathodic sites [9–11]." Due to the currently imposed environmental requirements for eco-friendly corrosion inhibitors, there is a growing interest in the use of natural products such as leaves or seeds extracts. The term "eco-friendly corrosion inhibitor" or "green inhibitor" refers to the substances that are biocompatible such as plant extracts since they are of biological origin. Thus, the natural products are being studied by several authors, for their corrosion inhibition potential as they are more environmentally friendly, showing good inhibition efficiency with the low risk of environmental pollution [12]. "Using of extracts of plant as inhibitors in acidic solutions, as *Nigella sativa* L.[13], *Apium graveolens* L. [14], *Glycyrrhiza glabra* [15], pomelo peel extract [16], *Dryopteris cochleata* leaf extracts [17], *Myrmecodia pendans* extract [18], *Morinda citrifolia* [19], *Thymus vulgaris* plant extract [20], *Mentha spicata* L. extract [21], phytoconstituent of *Ervatamia coronaria* [22], myrrh extract [23], *Cucurbita maxima* [24], *Adhatoda vasica*, *Eclipta alba* and *Centella asiatica* [25] have been investigated." *Prosopis juliflora* plays an important role in the ecological setup and economy of arid and semiarid environments as they play a vital role in sustainable development of the areas. It is known of reversal of desertification

✉ A. S. Fouda
asfouda@mans.edu.eg

[1] Chemistry Department, Faculty of Science, Mansoura University, El-Mansoura 35516, Egypt

and has been suggested as a miracle plant. Besides its use as a fuel plant, it has varied properties which are useful to the human kind. Every part of *P. juliflora* is abundantly being used in various fields. Extracts of *P. juliflora* seeds and leaves have several in vitro pharmacological effects such as antibacterial, antifungal and anti-inflammatory properties. It is also known for its ethno-medicinal properties, mainly used for boils, rheumatic pain, digestive disturbances. "Chemical studies have demonstrated that the PJF extract contains flavonoids such as apigenin, luteolin, apigenin 6,8-di-C-glycosides, chrysoeriol 7-*O*-glucoside, luteolin 7-*O*-glucoside, kaempferol 3-O-methyl ether, quercetin 3-*O*-methyl ether, isorhamnetin 3-*O*-glucoside, isorhamnetin 3-O-rutinoside, quercetin 3-*O*-rutinoside and quercetin 3-*O*-diglycoside (glucose, arabinose), alkaloids such as juliflorine, julifloricine and julifloridine, tannins and mineral elements such as Na, K, Ca, Cu, Fe, Zn and Mn" [26]. This study tests the PJF extract role on the dissolution mechanism of LCS in 1 M HCl acid medium. The PJF extract role is measured using gasometric method, mass loss method, polarization diagrams, EIS technique, SEM technique and AFM technique.

2 Experimental Techniques

2.1 Materials and Solutions

Corrosion tests have been worked on specimens of low-carbon steel with the chemical composition: 0.046% C, 0.900% Mn, 0.007% P, 0.002% Si and the remainder iron. The aggressive solution used was prepared by dilution of analytical reagent grade 34% HCl with bi-distilled water. The stock solution (1000 ppm) of PJF was used to prepare the desired concentrations by dilution with bi-distilled water.

3 Methods

3.1 Gasometric (GM) Method

The hydrogen evolution method is a useful technique that calculates the amount of hydrogen producing during a corrosion process. The used bottle must contact through a plastic tube to a burette. Initially, the air volume in the burette was measured. Finally, medium–low-carbon steel specimen was immersed in the test solution and the reaction bottle was enclosed. The amount of H_2 gas was measured by decreasing the aqueous solution level in the burette at fixed time intervals. Experiments were always repeated at least three times to check the reproducibility.

3.2 Mass Loss (ML) Method

Preweighed LCS sheets were suspended in 100 ml of 1 M HCl without and with the different contents of PJF extract ranging from 50 to 300 ppm. After different dipping time, the samples were outputted, washed with bi-distilled water, dried and weighted accurately. The inhibition efficiency (%IE) and the degree of surface coverage (θ) of the investigated inhibitors on the corrosion of LCS were calculated as follows [27]:

$$\mathrm{IE}\% = \theta \times 100 = \left[\left(W_{\mathrm{o}} - W\right)/W_{\mathrm{o}}\right] \times 100 \quad (1)$$

where W_{o} and W are the values of the average ML in the absence and presence of the inhibitor, respectively. Experiments were always performed at least three times to check the reproducibility.

3.3 Electrochemical Measurements

Electrochemical techniques were done using a typical three-compartment glass cell consisting of saturated calomel electrode (SCE) as a reference electrode and a platinum foil (> 1 cm^2) as a counter electrode. The steel specimen as working electrode was in the form of a square cut from steel sheet of equal composition embedded in epoxy resin of polytetrafluoroethylene so that the flat surface area was 1 cm^2. Prior to each measurement, the electrode surface was pretreated in the same manner as in the ML experiments. Before measurements, the electrode was immersed in solution at natural potential for 30 min until a steady state was reached.

3.3.1 Potentiodynamic Polarization (PP) Method

The potential was started from − 1000 to 0 mV vs open-circuit potential. All experiments were carried out in freshly prepared solutions at 25 °C.

3.3.2 Electrochemical Impedance Spectroscopy (EIS) Method

Impedance measurements were taken using AC signals of 5-mV peak-to-peak amplitude at the open-circuit potential in the frequency range of 100 kHz to 0.1 Hz. All impedance data were fitted to appropriate equivalent circuit using the Gamry Echem Analyst software. The experimental impedance was analyzed and interpreted on the basis of the equivalent circuit.

3.3.3 Electrochemical Frequency Modulation (EFM) Method

EFM experiments were performed with applying potential perturbation signal with amplitude 10 mV with two sine waves

of 2 and 5 Hz. The choice for the frequencies of 2 and 5 Hz was based on three arguments [28]. The larger peaks were used to calculate the corrosion current density (i_{corr}), the Tafel slopes (β_a and β_c) and the causality factors CF-2 and CF-3 [29]. Experiments were always carried out at least three times to check the reproducibility in all test methods.

All electrochemical measurements were taken using Gamry Instrument (PCI4/75 Potentiostat/Galvanostat/ZRA).

3.4 Scanning Electron Microscopy (SEM) Analysis

The surface morphology of the specimens was examined by SEM images recorded using the instrument VEGA3 TESCAN model.

3.5 Atomic Force Microscopy (AFM) analysis

The AFM images of polished, uninhibited and inhibited low-carbon steel samples were obtained using NanoSurf Easyscan 2 Flex AFM instruments (Nanotechnology Center, Mansoura University).

4 Results and Discussion

4.1 Hydrogen Evolution (HE) Method

The produced H_2 gas volume resulting from the corrosion reaction can be calculated. Results obtained by the HE method (in Fig. 1) are matching with other methods including MR and electrochemical methods. The hydrogen volume is dependent on the time of reaction according to Eq. (2):

$$V = Kt \tag{2}$$

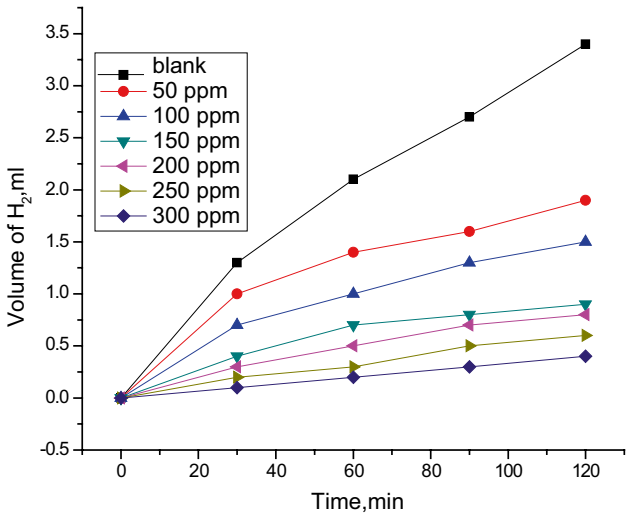

Fig. 1 Hydrogen evolution from LCS dissolution in 1 M HCl in the absence and presence of PJF extract at 25 °C

where V is the H_2 gas volume, t is time, and K is the corrosion rate. From Table 1, the results indicate that the extract decreased the H_2 gas volume and increased the protective percent [30]. From the volume of hydrogen evolved during the corrosion reaction, the corrosion rate (k_{corr}) was determined from Eq. (3)

$$k_{corr} = (Vt - Vi)/t_t - t_i \tag{3}$$

where Vt and Vi are the volumes of hydrogen evolved at time t_t and t_i, respectively. The results in Table 2 show that the corrosion rate decreased with the increase in PJF concentration. The %IE was determined using Eq. (4)

$$\%IE = [1 - (V_{Ht}/V^0_{Ht}) \times 100 \tag{4}$$

4.2 Mass Loss (ML) Measurements

The loss of mass of LCS is measured, at different time periods, without and with various extent of PJF extract. The relationship between mass reduction and time is shown in Fig. 2 for PJF extract. The corrosion inhibition efficiency is affected by the concentration of extract. The curves for different extract concentrations fell below the corrosive media. The increase in the concentration of the extract gives a decrease in the mass reduction and an increase in the metal corrosion protection. Experimental data show that the PJF extract is considered as

Table 1 %IE and k_{corr} of LCS obtained from gasometric method after 120 min in 1 M Hydrochloric acid for different PJF extract concentrations at 25 °C

[Inh] (ppm)	Volume of hydrogen gas evolved (ml)	$k_{corr} \times 103$ (ml/min)	%IE
Blank	3.4	28.3	–
50	1.9	15.8	44.1
100	1.5	12.5	55.9
150	0.9	7.5	73.5
200	0.8	6.7	76.5
250	0.6	5	82.4
300	0.4	3.3	88.2

Table 2 %IE and θ of PJF extract for the LCS dissolution in hydrochloric acid from ML data at various concentrations of PJF extract at 25 °C

[inh.] (ppm)	Prosopis extract	
	%IE	θ
50	57.6	0.576
100	65.8	0.658
150	68.3	0.683
200	69.1	0.691
250	71.1	0.711
300	72.6	0.726

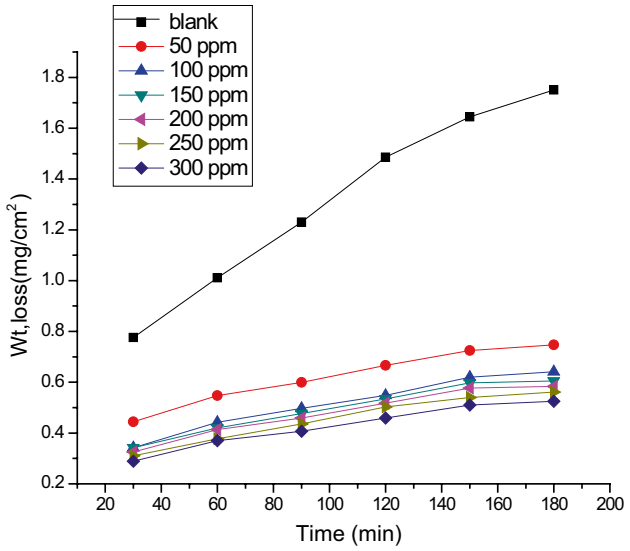

Fig. 2 Curves of ML versus time for the corroded LCS in 1 M hydrochloric acid without and with the various PJF solution concentrations at 25 °C

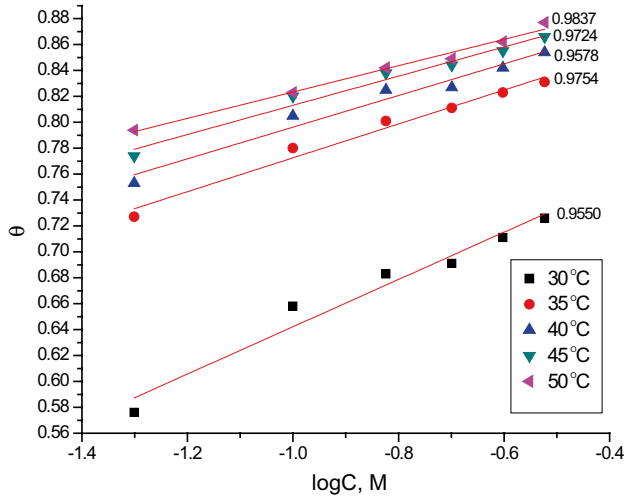

Fig. 3 Diagram of Temkin adsorption of PJF plant extract on the surface of LCS in 1 M HCl at different temperatures

inhibitory substance for LCS corrosion in 1 M HCl medium. Also, the (Θ) and %IE due to the thin layer, founded by Eq. (1), rise with rising the extract extents. The data are given in Table 2.

4.3 Adsorption Isotherms

Temkin equation which is represented in Fig. 3 is used to calculate θ for PJF extract. The covered surface area (θ) was calculated at several extract contents in 1 M hydrochloric acid media. The best fitting obeys the Temkin adsorption isotherm [31].

$$\Theta_{\text{coverage}} = (2.303/a)\,\text{Log}\,C + (2.303/a)\,\text{Log}\,K_{\text{ads}} \quad (5)$$

where K_{ads} is the adsorption constant, C is the concentration (mol l^{-1}) of the extract, and "a" is heterogeneous factor of metal surface. The values of "a," K_{ads} and $\Delta G^{\text{o}}_{\text{ads}}$ obtained are given in Table 3.

The K_{ads} is utilized to calculate the adsorption energy of $\Delta G^{\text{o}}_{\text{ads}}$ as follows:

$$K_{\text{ads}} = \frac{1}{55.5}\exp\left[\frac{-\Delta G^{\text{o}}_{\text{ads}}}{RT}\right] \quad (6)$$

From Table 3, $\Delta G^{\text{o}}_{\text{ads}}$ depends on temperature. The positive values of $\Delta G^{\text{o}}_{\text{ads}}$ indicate that the extract was adsorbed spontaneously on the metal surface. From $\Delta G^{\text{o}}_{\text{ads}}$ values, the adsorption of the PJF components is mixed one, but mainly chemisorbed. Positive value of (a) showed attractive forces between adsorbed molecules [32] on the LCS surface. Large values of K_{ads} modify more effective adsorption and hence higher protective effective [33]. K_{ads} values that are raised with the rise in temperature indicate that the PJF extract is mainly chemically adsorbed onto the LCS surface. The high values of $\Delta H^{\text{o}}_{\text{ads}}$ indicate the chemisorption type [34]. From the LCS van't Hoff equation,

$$\text{Log}\,K_{\text{ads}} = \left(-\Delta H^{\text{o}}_{\text{ads}}/2.303\,RT\right) + \text{constant} \quad (7)$$

$\Delta H^{\text{o}}_{\text{ads}}$ can be also deduced from the plot of log K_{ads} versus $1/T$ giving straight lines with slopes of $\Delta H^{\text{o}}_{\text{ads}}/R$ (Fig. 4).

From Fig. 5, the entropy of adsorption can be measured from Eq. (8):

$$\Delta G^{\text{o}}_{\text{ads}} = \Delta H^{\text{o}}_{\text{ads}} - T\,\Delta S^{\text{o}}_{\text{ads}} \quad (8)$$

Table 3 Some parameters from Temkin isotherm for LCS in 1 M hydrochloric acid for PJF plant extract at 25 °C

Temp. (K)	$K_{\text{ads}} \times 10^{-6}$ (M^{-1})	a	$-\Delta G^{\text{o}}_{\text{ads}}$ (kJ mol^{-1})	$-\Delta H^{\text{o}}_{\text{ads}}$ (kJ mol^{-1})	$-\Delta S^{\text{o}}_{\text{ads}}$ (J mol^{-1} k^{-1})
303	0.03	12.6	36.3	411	1476
308	2.6	16.4	48.1		1491
313	33.1	18.9	55.5		1490
318	165.9	20.5	60.7		1483
323	1258.9	22.7	67.1		1480

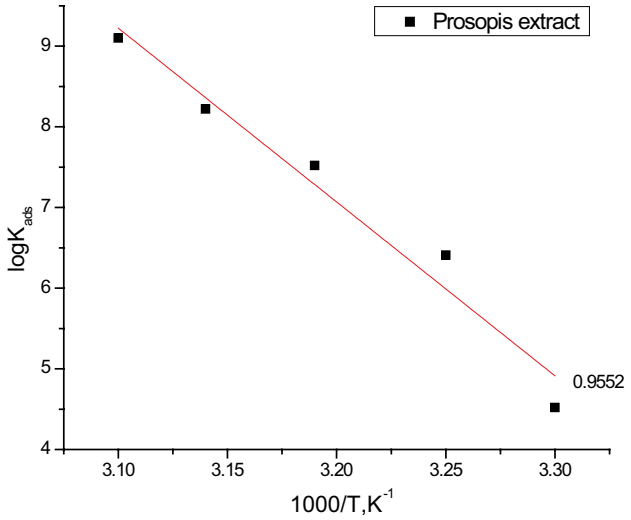

Fig. 4 Log K_{ads} versus $1/T$ for the corrosion of LCS in the presence of PJF extract

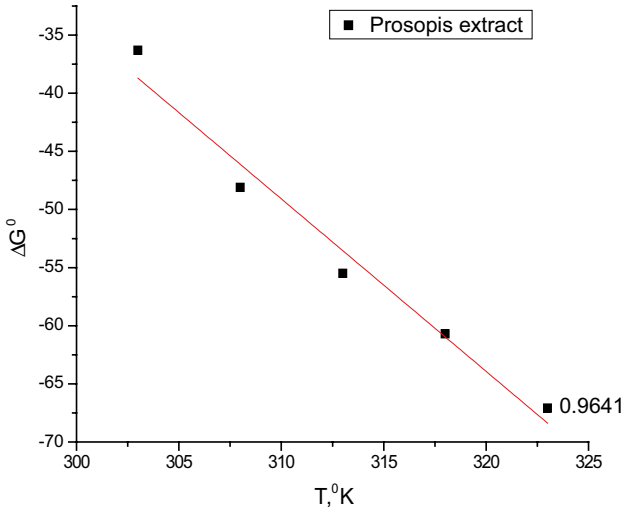

Fig. 5 ΔG^{o}_{ads} versus T for the corrosion of LCS in the presence of PJF extract

The calculated ΔH^{o}_{ads} and ΔS^{o}_{ads} are given in Table 3. The data showed that the calculated ΔH^{o}_{ads} values are positive which indicate that the adsorption process is endothermic. The higher and positive values of ΔS^{o}_{ads} indicate that the small molecules or ions such as H_2O, Cl^- which interact with the surface atoms of LCS are replaced by PJF extract molecules that raise the disorder of the medium [35].

4.4 Effect of Temperature

The corrosion rate of LCS in 1 M HCl and with concentrations of PJF extract was tested in the range of temperature from 303 to 323 K by ML method (Fig. 6). From Table 4, both of the rate of k_{corr} and %IE for PJF extract were increased by raising temperature. The increase in %IE with raising the temperature proves that at low temperatures the extract is physisorbed, but at high temperature is chemisorbed [36, 37].

4.5 Activation Studies

The dissolution reaction parameters were measured from the equation of Arrhenius (9):

$$\text{Log } k_{corr} = -E^{*}_{a}/2.303\,RT + \log A \tag{9}$$

where R is universal gas constant, E^{*}_{a} is energy of activated complex, T is Kelvin's temperature, and A is Arrhenius factor. From Table 5, the magnitude of E^{*}_{a} for the metal in corrosive medium in the absence and presence of different PJF extract concentrations calculated from drawing k_{corr} Logarithm against temperature reciprocal plots is shown in Fig. 7. Table 5 shows that the E^{*}_{a} decreases in the occurrence of PJF due to the delayed rate of adsorption with a resultant closer approach to equilibrium during the experiments at higher temperatures according to Hoar and Holliday [38]. "But, Riggs and Hurd [39] explained that the reduction in the activation energy of corrosion at higher levels of inhibition arises from a shift of the net corrosion reaction from the uncovered part of the metal surface to the covered one". For the activated complex, the enthalpy change (ΔH^{*}) and entropy change are calculated from Eq. (10):

$$k_{corr} = (RT/Nh)\exp(\Delta S^{*}/R)\exp(-\Delta H^{*}/RT) \tag{10}$$

where k_{corr} is the metal corrosion rate, h is Planck's constant, and N is Avogadro's number. Figure 8 indicates a draw of

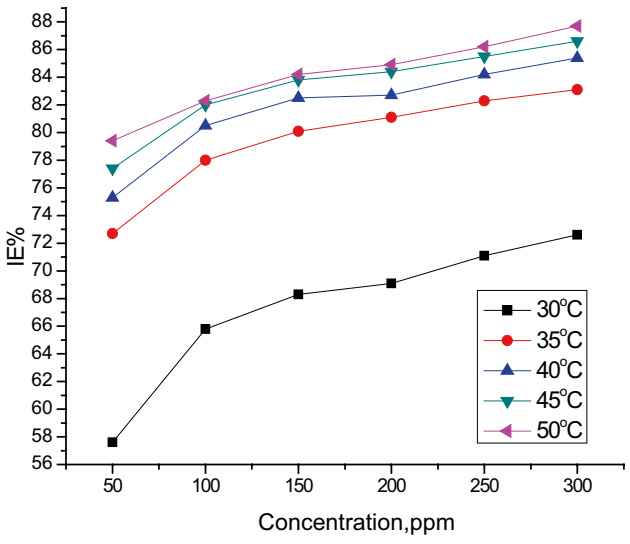

Fig. 6 Effect of concentration and temperature on the %IE of PJF extract

Table 4 Data of %IE, (θ) and (k_{corr}) in hydrochloric acid using ML method with different PJF extract concentrations at various temperatures

Conc. (ppm)	Temp. (°C)	k_{corr} (mg cm^2 min^{-1})	θ	%IE
1 M HCl	30	12	–	–
	35	22	–	–
	40	32	–	–
	45	37	–	–
	50	48	–	–
50	30	5.3	0.576	57.6
	35	6.1	0.727	72.7
	40	7.8	0.753	75.3
	45	11.1	0.774	77.4
	50	13.8	0.794	79.4
100	30	4.3	0.658	65.8
	35	4.9	0.78	78
	40	6.2	0.805	80.5
	45	8.8	0.82	82
	50	9.4	0.823	82.3
150	30	4	0.824	82.4
	35	4.4	0.825	82.5
	40	5.6	0.827	82.7
	45	8	0.838	83.8
	50	8.4	0.842	84.2
200	30	3.9	0.691	69.1
	35	4.2	0.811	81.1
	40	5.5	0.827	82.7
	45	7.7	0.844	84.4
	50	8	0.849	84.9
250	30	3.6	0.711	71.1
	35	4	0.823	82.3
	40	5	0.842	84.2
	45	7.1	0.855	85.5
	50	7.3	0.862	86.2
300	30	3.4	0.726	72.6
	35	3.8	0.831	83.1
	40	4.7	0.854	85.4
	45	6.6	0.866	86.6
	50	6.8	0.877	87.7

log k_{corr}/T versus $1/T$ with PJF extract in hydrochloric acid. Straight lines are given (slopes = ($\Delta H^*/2.303\ R$) and intercepts are [log ($R/Nh + \Delta S^*/2.303\ R$)] written in Table 5.

The activation energy decreases with the increase in the extract content (Table 5), and then, the adsorption is chemical type. The positive ΔH^* indicates the extract adsorption is endothermic. The negative $\Delta S^*$with and without the extract shows that in the rate-determining step, the association of unstable coordinated compound is more than the dissociation [40].

Table 5 Kinetic parameters for activated state of LCS without and with PJF extract concentrations in 1 M hydrochloric acid

Conc. (ppm)	Activation parameters		
	E^*a (kJ mol^{-1})	ΔH^* (kJ mol^{-1})	$-\Delta S^*$ (J mol^{-1}K^{-1})
Blank	50.6	48.0	121.6
50	40.7	38.1	163.3
100	33.5	30.9	188.6
150	31.9	29.3	194.7
200	31.5	28.9	196.2
250	30.4	27.8	200.4
300	29.1	26.5	205.0

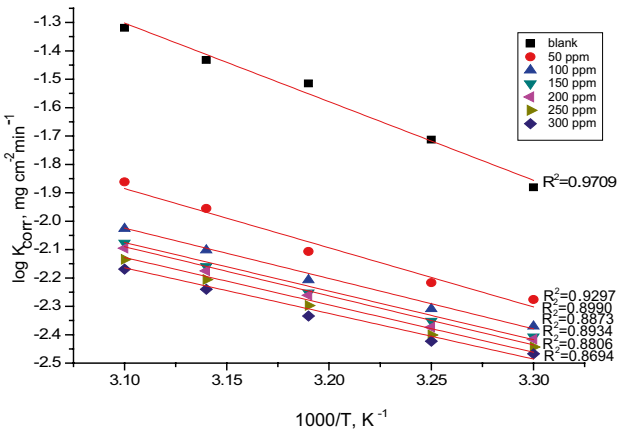

Fig. 7 Diagram of Arrhenius ($1/T$ versus log k_{corr}) for dissolution of LCS in 1 M HCl without and with different PJF extract concentrations

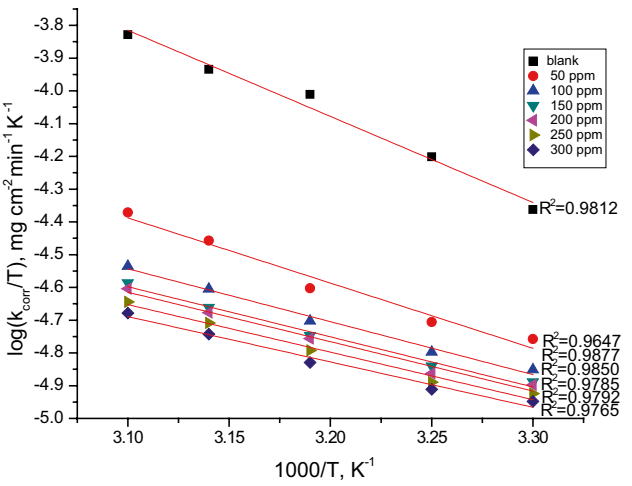

Fig. 8 Diagram of (log k_{corr}/T) versus $1/T$ for dissolution of LCS in hydrochloric acid without and with different PJF extract concentrations

4.6 Electrochemical Frequency Modulation Technique (EFM)

EFM is safe dissolution method that identified the current magnitude without meaningful Tafel constants, and with only a small signal of polarizing [41]. Figure 9 shows the EFM spectrum of LCS in hydrochloric acid solution with various PJF extract contents. From Table 6, the addition of PJF extract with different concentrations to the corrosive medium reduces the current density of corrosion, meaning that PJF extract acts as inhibitor by adsorption process. The causality factors are very closer to theoretical values which according to EFM theory [42] should prove the validity of Tafel slopes and corrosion current densities. $\%IE_{EFM}$ raises by rising contents of extract, and it can be measured using Eq. (11):

$$\%IE_{EFM} = \left[1 - \left(i_{corr}/i^{o}_{corr}\right)\right] \times 100 \quad (11)$$

where i^{o}_{corr} and i_{corr} are corrosion current densities without and with extract, respectively.

4.7 Electrochemical Impedance Spectroscopy (EIS) Tests

Figure 10 indicates the resistance curves for LCS in 1 M hydrochloric acid medium without and with PJF extract. The Nyquist plots do not produce perfect semicircles due to the irregularity of frequency [43] resulting from the surface asymmetry and the roughness of the surface. "The

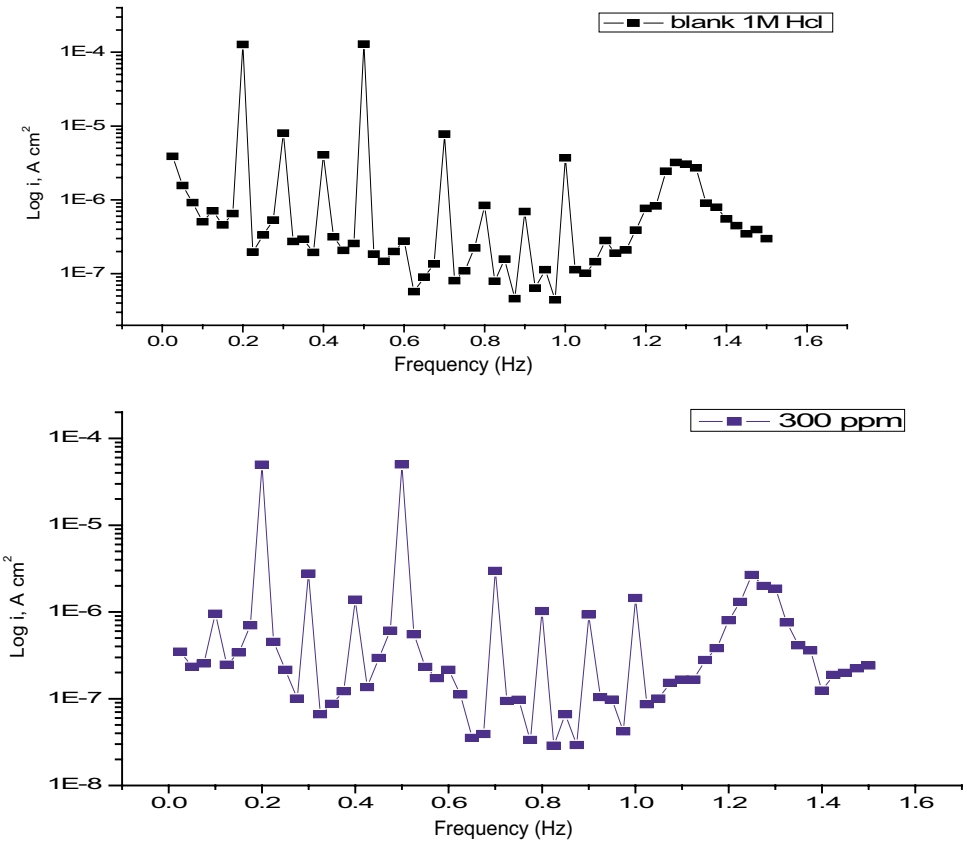

Fig. 9 EFM spectrums for the dissolution of LCS in 1 M HCl without and with various PJF extract extent

Table 6 EFM parameters for LCS in the absence and presence of various PJF concentrations in 1 M HCl at 25 °C

[inh] (ppm)	i_{corr} (μA cm^{-2})	β_c (mV dec^{-1})	β_a (mV dec^{-1})	CF-2	CF-3	k_{corr} (mpy)	Θ	%IE
Blank	354.2	275.4	134.5	2.06	2.44	161.8	–	–
50	252.6	97.0	82.4	1.93	2.86	115.4	0.287	28.7
100	234.8	98.6	82.4	1.91	2.98	107.3	0.337	33.7
150	104.7	97.7	76.0	1.81	3.50	47.8	0.704	70.4
200	98.7	108.2	78.0	2.13	3.20	45.1	0.721	72.1
250	74.0	90.4	67.7	2.04	3.60	33.8	0.791	79.1
300	67.0	103.4	75.7	2.03	4.07	30.6	0.811	81.1

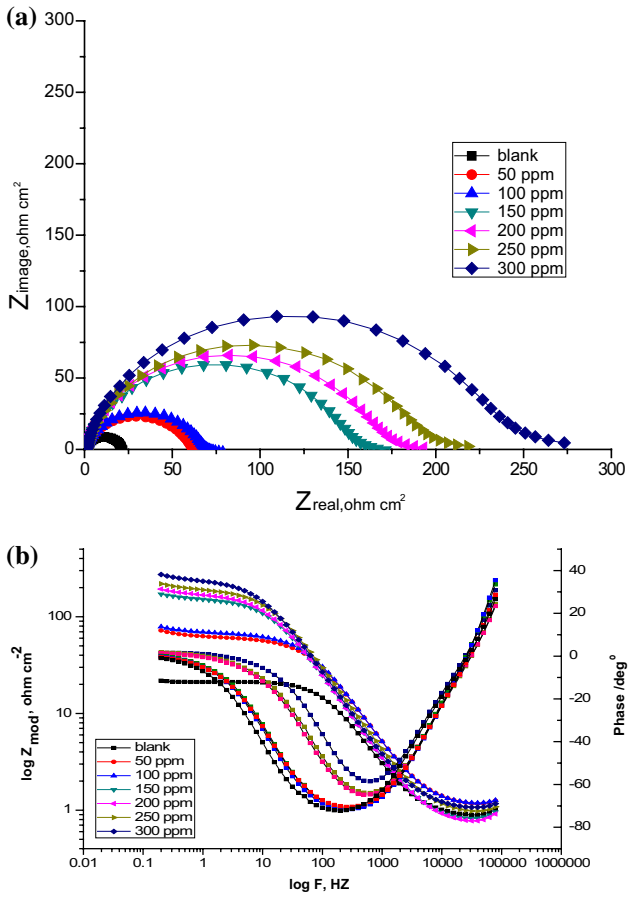

Fig. 10 **a** Nyquist diagram for the LCS dissolution in hydrochloric acid without and with PJF extract concentrations at 25 °C. **b** The Bode diagram for the LCS dissolution in hydrochloric acid without and with various PJF extract concentrations at 25 °C

semicircular shape shows that the corrosion of LCS is controlled by the charge transfer and the presence of PJF does not change the mechanism of LCS dissolution" [44]. The addition of PJF raises the R_{ct} value in corrosive medium. The C_{dl} reduces with the increase in PJF concentration. These results prove the occurrence of a protective adsorbed layer.

Figure 11 shows the equivalent electrical circuit utilized for fitting the results. The C_{dl}, Y_0 and n were measured by Eq. (12) [45]:

$$C_{dl} = Y_0 \omega^{n-1} / \sin[n(\pi/2)] \quad (12)$$

where Y_0 is the CPE value, $\omega = 2\pi f_{max}$, f_{max} is the angular frequency, and n is the exponential. From Table 7, the CPE/C_{dl} decreases with a decrease in dielectric factor and/or to an increase in the double-layer thickness, advising that the extract components are adsorbed at the metal/solution interface [46]. The %IE can be measured from Eq. (13) [47]:

$$\%IE_{EIS} = \left[1 - \left(R_{ct}^{o}/R_{ct}\right)\right] \times 100 \quad (13)$$

where R_{ct}^{o} and R_{ct} are the resistance of charge moving values in extract free and inhibitory solution, respectively.

The Bode plot (Fig. 10b) shows single maximum at intermediary frequencies, broadening of this maximum in the presence of PJF extract resulting from the formation of a protective film onto the low-carbon steel surface. The higher values of both phase angle and impedance for inhibitory solutions than uninhibited solution reproduce the inhibition effect of PJF extract. Additionally, these values rise on the rise in the concentration of studied extract [48].

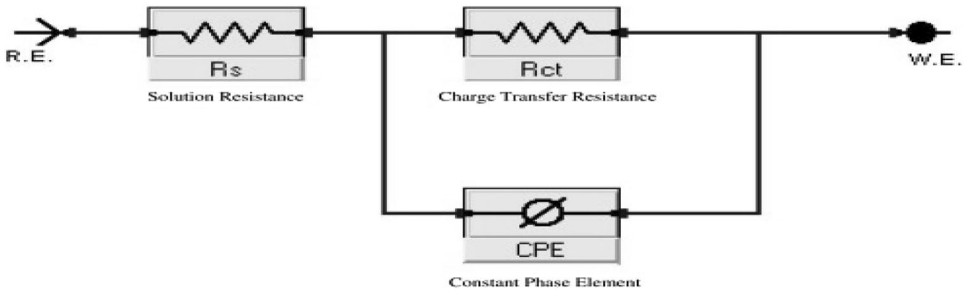

Fig. 11 Equivalent circuit for fitting EIS data for LCS in 1 M hydrochloric acid solutions

Table 7 Parameters measured by EIS method for LCS in 1 M hydrochloric acid without and with PJF extract concentrations at 25 °C

[inh.] (ppm)	R_S (Ω cm^2)	Y^o (μΩ^{-1} s^n cm^{-2})	n	R_{ct} (Ω cm^2)	C_{dl} (μF cm^{-2})	Θ	%IE
0.0	0.906	460.8	0.922	20.2	310.4	–	–
50	1.168	83.7	0.920	60.1	52.8	0.664	66.4
100	1.179	82.5	0.918	66.7	51.9	0.697	69.7
150	0.814	81.8	0.903	150.5	51.0	0.866	86.6
200	0.772	80.7	0.900	168.5	50.3	0.880	88.0
250	0.970	79.7	0.890	190.7	47.5	0.894	89.4
300	1.071	78.3	0.886	238.5	46.9	0.915	91.5

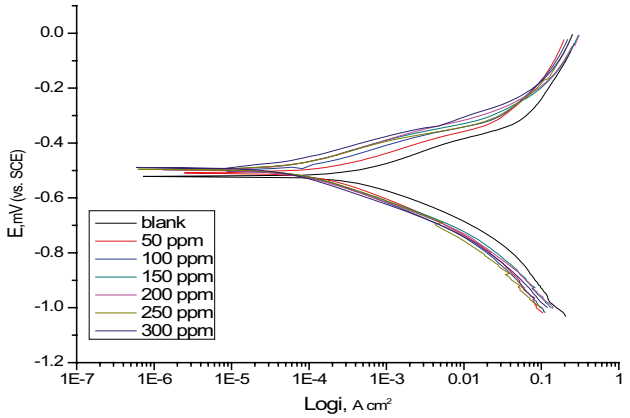

Fig. 12 Corrosion polarization plots for the LCS in 1 M hydrochloric acid without and with PJF extract concentrations at 25 °C

4.8 Potentiodynamic Polarization Curves

Figure 12 shows the polarization curves for LCS corrosion in one molar hydrochloric acid with and without PJF extract extent at 25 °C. The protective percent and covered surface area are measured from Eq. (14):

$$\%\mathrm{IE}_p = \left[\left(i^{\mathrm{o}}_{\mathrm{corr}} - i_{\mathrm{corr}}\right)/i^{\mathrm{o}}_{\mathrm{corr}}\right] \times 100 = \theta \times 100 \qquad (14)$$

where i_{corr} and i_{corr} are the free and inhibited current densities, respectively. From Table 8, the decrease in i_{corr} is clearly with the increase in the inhibitor concentration. The maximum displacement in E_{corr} is < 85 mV/E_{corr}, which considers that the PU affects the reaction of both anodic and cathodic [49]. Additionally, this extract causes no change in the Tafel slopes, signifying that this extract is firstly adsorbed onto metal surface and therefore resist by only blocking the active positions with no change in the reaction mechanism [50].

4.9 Scanning Electron Microscopy (SEM) Analysis

Surface morphology of LCS was evaluated by scanning electron microscopy after 24-h dipping in 1 M HCl before and after the addition of inhibitor. The SEM micrograph of Fig. 13a represents the smooth surface of LCS, while Fig. 13b shows powerfully damaged steel surface due to the dissolution after dipping in 1 M HCl. SEM image of low-carbon steel surface after immersion in 1 M HCl and 300 ppm PJF is shown in Fig. 13c. However, in the presence of 300 ppm PJF, the LCS surface coverage increases, proposing formation of a protective inhibitory layer at the surface of LCS.

Table 8 Dissolution voltage (E_{corr}), current density (i_{corr}), Tafel constants (β_{c}, β_{a}) and (θ), and protective percent ($\%\mathrm{IE}_{\mathrm{p}}$) of LCS in hydrochloric acid at room temperature for PJF extract

[inh] (ppm)	$-E_{\mathrm{corr}}$ (mV vs. SCE)	i_{corr} (μA cm^{-2})	β_{c} (mV dec^{-1})	β_{a} (mV dec^{-1})	k_{corr} (mpy)	θ	%IE
Blank	522	375.0	114.0	96.3	171.3	–	–
50	509	169.0	127.6	87.6	77.3	0.549	54.9
100	501	87.4	114.2	81.1	39.9	0.767	76.7
150	496	63.1	102.1	81.6	28.8	0.832	83.2
200	498	62.5	103.3	86.8	28.6	0.833	83.3
250	495	52.8	92.2	72.8	24.1	0.859	85.9
300	488	34.9	93.7	75.7	16.0	0.907	90.7

Fig. 13 SEM micrographs of **a** polished LCS, **b** low-carbon steel immersed in 1 M HCl, **c** LCS immersed in1 M HCl containing 300 ppm PJF

4.10 Atomic Force Microscopy (AFM) Analysis

AFM provides images with atomic or near-atomic-resolution surface topography, capable of computing surface roughness of samples. The three-dimensional (3D) AFM morphologies for polished LCS surface and LCS surface in 1 M HCl with and without PJF extract are shown in Fig. 14.

From Table 9, the data suggest that low-carbon steel surface immersed in 1 M HCl has a greater surface roughness than the polished metal surface, which shows that LCS sample is severely scratched due to the acid attack. The roughness average of protected LCS was reduced to 250.4 nm. These parameters confirm that the surface is smoother. The smoothness of the surface is due to the formation of a

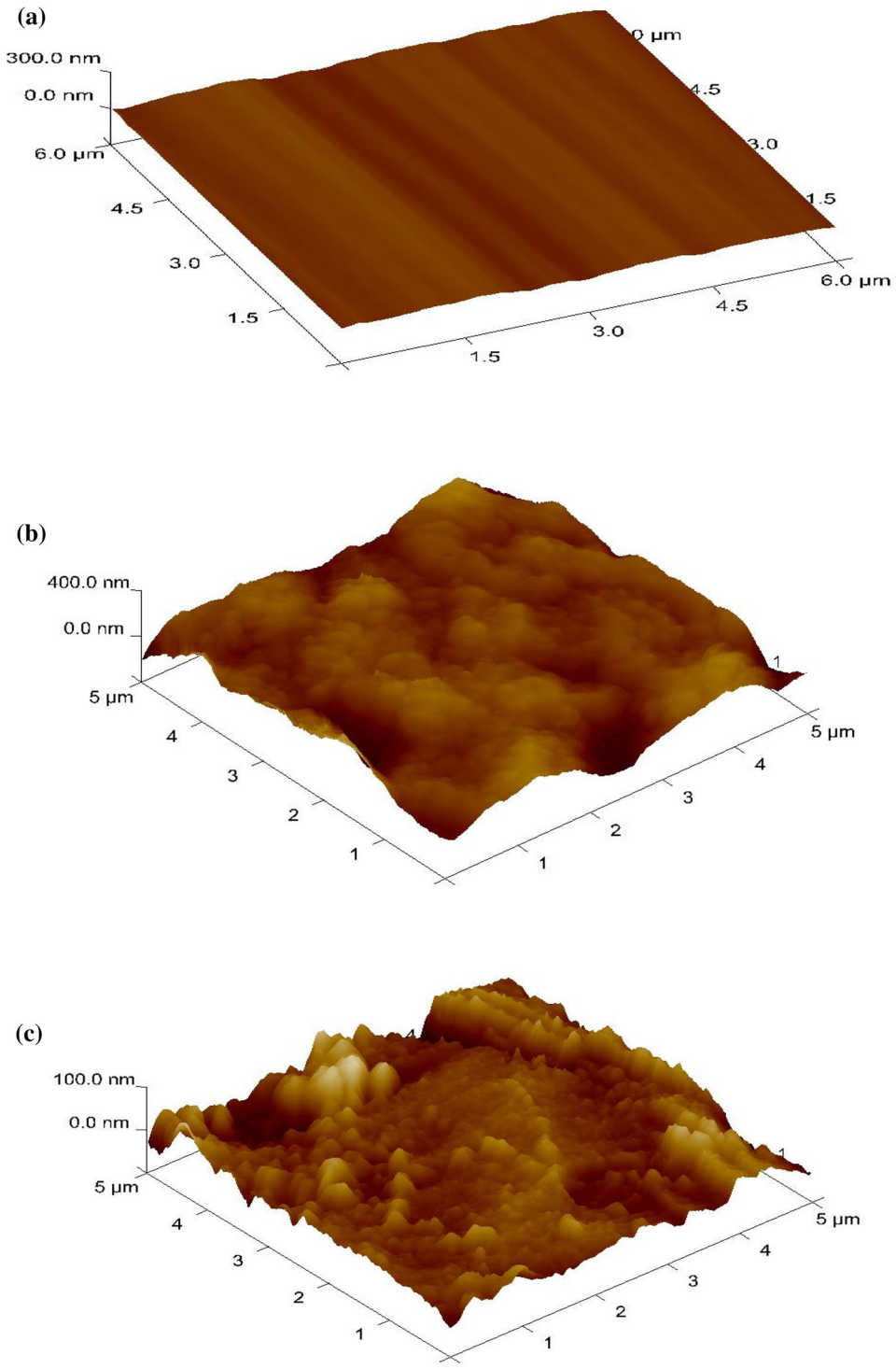

Fig. 14 Three-dimensional AFM images of the surface of **a** as-polished LCS; **b** LCS immersed in 1 M HCl; **c** LCS immersed in 1 M HCl containing PJF (300 ppm)

Table 9 AFM data for LCS surface dipped in inhibited and uninhibited media

Samples	The root mean square (nm)	Roughness average (nm)	The peak-valley height (nm)
Polished LCS	18.1	14.1	99.1
LCS in 1 M HC	493.2	392.6	4699.8
LCS in 1 M HCl + 300 ppm PJF	359.2	250.4	2894.9

compacted protective film of extract on the metal surface, thereby preventing the corrosion of LCS [51].

4.11 Mechanism of Corrosion Inhibition

According to electrochemical measurements, the addition of PJF extract leads to retarding the LCS corrosion. From the results, the mechanism of inhibition involves blocking of surface active sites by adsorption of PJF molecules. The adsorption mechanism of PJF extract on the LCS surface involves a physisorption. Phytochemical analysis of PJF extract indicates the existence of flavonoids, alkaloids, carbohydrates, phenols, tannins. These components have heteroatoms such as –N, –O, which strongly was adsorbed onto a LCS surface. The inhibitive effect of these components may be recognized to their adsorption via the –NH, C=O, OH, etc., groups and also the presence of π-electrons in the rings. These organic molecules get adsorbed on the metal surface, forming a protective film, and therefore, the inhibition occurs [52].

5 Conclusions

PJF extract has corrosion inhibitory effect on LCS in hydrochloric acid medium. Polarization plots data mention that the PJF extract is mixed-type inhibitor. Corrosion protection efficiencies of PJF extract rise with the rise in temperature, but the energy of corrosion activation was decreased (chemisorption). The adsorption of PJF extract follows the Temkin adsorption isotherm. SEM and AFM techniques give information about morphology, topography and the roughness of the metal surface. There is good agreement between chemical and electrochemical techniques.

References

1. Li LF, Caenen P, Celis JP (2008) Effect of hydrochloric acid on pickling of hot-rolled 304 stainless steel in iron chloride-based electrolytes. Corros Sci 50:804–810
2. Quraishi MA, Sardar R (2002) Aromatic triazoles as corrosion inhibitors for low carbon steel in acidic environments. Corrosion 58:748–755
3. Karakus M, Sahin M, Bilgic S (2005) an investigation on the inhibition effects of some new dithiophosphonic acid monoesthers on the corrosion of the steel in 1 M HCl medium. Mater Chem Phys 92:565–571
4. Sherif EM, Park SM (2006) Inhibition of copper corrosion in acidic pickling solutions by *N*-phenyl-1,4-phenylenediamine. Electrochim Acta 51:4665–4673
5. Zucchi F, Omar IH (1985) Plant extracts as corrosion inhibitors of mild steel in HCl solutions. Surf Technol 24(4):391–399
6. Gunasekaran G, Chauhan LR (2004) Eco friendly inhibitor for corrosion inhibition of mild steel in phosphoric acid medium. Electrochim Acta 49:4387–4395
7. Li Y, Zhao P, Liaqng Q, Hou B (2005) Berberine as a natural source inhibitor for mild steel in 1 M H_2SO_4. Appl Surf Sci 252:1245–1253
8. El-Etre AY, Abdallah M, El-Tantawy ZE (2005) Corrosion inhibition of some metals using lawsonia extract. Corros Sci 47:385–395
9. El-Etre AY (2006) extract as inhibitor for acid corrosion of SX 316 steel. Appl Surf Sci 252:8521–8525
10. Orubite KO, Oforka NC (2004) Inhibition of the corrosion of mild steel in hydrochloric acid solutions by the extracts of leaves of *Nypafruticans* Wurmb. Mater Lett 58:1768–1772
11. Avwiri GO, Igho FO (2001) Inhibitive action of *Vernonia amygdalina* on the corrosion of aluminum alloys in acidic media. Mater Lett 57:3705–3711
12. Boujakhrout A, Hamdani I, Krim O, Bouyanzer A, Santana RV, Zarrouk A, Hammouti B, Oudda H (2016) *Kimbiolongo* extract as corrosion inhibitor for mild steel in 1.0 M HCl. Der Pharmacia Lettre 8(2):180–187
13. Al-Moubaraki AH, Al-Howiti AA, Al-Dailami MM, Al-Ghamdi EA (2017) Role of aqueous extract of celery (*Apium graveolens* L.) seeds against the corrosion of aluminum/sodium hydroxide systems. J Environ Chem Eng 5(5):4194–4205
14. Koundal V, Haldhar R, Saxena A, Prasad D (2017) AIP natural nonpoisonous green inhibitor of *Glycyrrhiza glabra* for mild steel in 3.5% NaCl. In: Conference proceedings, 1860, 020063
15. Sun Z, Singh A, Xu X, Liu W, Lin Y (2017) Inhibition effect of pomelo peel extract for N80 steel in 3.5% NaCl saturated with CO_2 solution. Res Chem Intermed 43:1–18
16. Nathiya RS, Raj V (2017) Evaluation of *Dryopteris cochleata* leaf extracts as green inhibitor for corrosion of aluminum in 1 M H_2SO_4. Egypt J Pet 26(2):313–323
17. Pradityana A, Sulistijono, Winarto, Luwar B, Mursid, M (2017) Effect of temperature on the application of *Myrmecodia pendans* extract for environmentally friendly corrosion inhibitor. In: AIP CONFERENCE proceedings, 1840, 030001
18. Kusumastuti R, Pramana RI, Soedarsono JW (2017) The use of *Morinda citrifolia* as a green corrosion inhibitor for low carbon steel in 3.5% NaCl solution. In: AIP Conference proceedings 1823, 020012
19. Ehsani A, Mahjani MG, Hosseini M, Moshrefi R, Mohammad Shiri H (2017) Evaluation of Thymus vulgaris plant extract as an eco-friendly corrosion inhibitor for stainless steel 304 in acidic solution by means of electrochemical impedance spectroscopy, electrochemical noise analysis and density functional theory. J Colloid Interface Sci 490:444–451
20. Shahidi M, Golestani G, Gholamhosseinzadeh MR (2017) *Mentha spicata* L. extract as a green corrosion inhibitor for carbon steel in HCl solution. Phys Chem Res 5(2):293–307
21. Sethuraman MG, Aishwarya V, Kamal C, Jebakumar Immanuel Edison T (2017) Studies on Ervatinine—the anticorrosive phytoconstituent of *Ervatamia coronaria*. Arab J Chem 10:S522–S530

22. Gadow HS, Motawea MM, Elabbasy HM (2017) Investigation of myrrh extract as a new corrosion inhibitor for α-brass in 3.5% NaCl solution polluted by 16 ppm sulfide. RSC Adv 7(47):29883–29898
23. Anbarasi K, Vasudha VG (2017) Influence of ecofriendly plant material (*Cucurbita maxima*) on mild steel corrosion. Anti-Corros Methods Mater 64(5):492–498
24. Shyamala M, Arulanantham A (2017) A comparative study on the inhibitory action of some green inhibitors on the corrosion of mild steel in hydrochloric acid medium. Malays J Anal Sci 21(2):346–355
25. Venegas R, Figueredo F, Carvallo G, Molinari A, Vera R (2016) Evaluation of *Eulychnia acida* Phil. (Cactaceae) extracts as corrosion inhibitors for carbon steel in acidic media. Int J Electrochem Sci 11:3651–3663
26. Dave PN, Bhandari J (2013) *Prosopis julifera*: a review. Int J Chem Stud 1(3):181–196
27. El-Etre AY (2008) Inhibition of C-steel corrosion in acidic solution using the aqueous extract of zallouh root. Mater Chem Phys 108:278–282
28. Bosch RW, Hubrecht J, Bogaerts WF, Syrett BC (2001) Electrochemical frequency modulation: a new electrochemical technique for online corrosion monitoring. Corrosion 57:60–70
29. Abdel-Rehim SS, Khaled KF, Abd-Elshafi NS (2006) Electrochemical frequency modulation as a new technique for monitoring corrosion inhibition of iron in acid media by new thiourea derivative. Electrochim Acta 51:3269–3277
30. Bockris JOM, Drazic D (1962) the kinetics of deposition and dissolution of iron: effect of alloying impurities. Electrochim Acta 7(3):293–313
31. Frumkin AN (1963) Hydrogen overvoltage and adsorption phenomena. In: Delahay P, Tobias CW (eds) Advances in electrochemistry and electrochemical engineering, vol 3, chapter 5. Interscience Publisher Inc., New York
32. Noor EA (2007) Temperature effects on the corrosion inhibition of mild steel in acidic solutions by aqueous extract of Fenugreek leaves. Int J Electrochem Sci 2:996–1017
33. Refray SAM, Taha F, Abd El-Malak AM (2004) Inhibition of stainless steel pitting corrosion in acidic medium by 2-mercaptobenzoxazole. Appl Surf Sci 236:175–185
34. Durnie W, Marco RD, Jefferson A, Kinsella B (1999) Development of a structure-activity relationship for oil field corrosion inhibitors. J Electrochem Soc 146:1751–1756
35. Li L, Qu Q, Bai W, Yang F, Chen Y, Zhang S, Ding Z (2012) Sodium diethyldithiocarbamate as a corrosion inhibitor of cold rolled steel in 0.5 M hydrochloric acid solution. Corros Sci 59:249–257
36. Umoren SA, Obot IB, Ebenso EE, Okafor PC, Ogbobe O, Oguzie EE (2006) Gum arabic as a potential corrosion inhibitor for aluminium in alkaline medium and its adsorption characteristics. Anti Corros Meth Mater 53:277–282
37. Abdallah M (2004) Antibacterial drugs as corrosion inhibitors for corrosion of aluminium in hydrochloric solution. Corros Sci 46(8):1981–1996
38. Hour TP, Holliday RD (1953) the inhibition by quinolines and thioureas of the acid dissolution of mild steel. J Appl Chem 3:502–513
39. Riggs LO Jr, Hurd TJ (1967) Temperature coefficient of corrosion inhibition. Corrosion 23(8):252–260
40. Afak SS, Duran B, Yurt A, Turkoglu G (2012) Schiff bases as corrosion inhibitor for aluminium in HCl solution. Corros Sci 54:251–259
41. Kus E, Mansfeld F (2006) an evaluation of the electrochemical frequency modulation (EFM) technique. Corros Sci 48(4):965–979
42. Abdel Nazeer A, Allam NK, Fouda AS, Ashour EA (2012) Effect of cysteine on the electrochemical behavior of Cu10Ni alloy in sulfide polluted environments: experimental and theoretical aspects. Mater Chem Phys 136:1–9
43. El Achouri M, Kertit S, Gouttaya HM, Nciri B, Bensouda Y, Perez L, Infante MR, Elkacemi K (2001) Corrosion inhibition of iron in 1 M HCl by some gemini surfactants in the series of alkanediyl-α, ω-bis-(dimethyl tetradecyl ammonium bromide). Prog Org Coat 43(4):267–273
44. Shalabi K, Abdel Nazeer A (2015) Adsorption and inhibitive effect of *Schinus terebinthifolius* extract as a green corrosion inhibitor for carbon steel in acidic solution. Prot Met Phys Chem Surf 51(5):908–917
45. Mertens SF, Xhoffer C, Decooman BC, Temmerman E (1997) Short-term deterioration of polymer-coated 55% Al–Zn. 1. Behavior of thin polymer films. Corrosion 53(5):381–388
46. Ghareba S, Omanovic S (2011) 12-Aminododecanoic acid as a corrosion inhibitor for carbon steel. Electrochim Acta 56(11):3890–3898
47. Ma H, Chen S, Niu L, Zhao S, Li S, Li D (2002) Inhibition of copper corrosion by several Schiff bases in aerated halide solutions. J Appl Electrochem 32(1):65–72
48. Yadav M, Kumar S, Kumari N, Bahadur I, Ebenso EE (2015) Experimental and theoretical studies on corrosion inhibition effect of synthesized benzothiazole derivatives on mild steel in 15% HCl solution. Int J Electrochem Sci 10:602–624
49. El Faydy M, Galai M, El Assyry A, Tazouti A, Touir R, Lakhrissi B, Ebn Touhami M, Zarrouk A (2016) Experimental investigation on the corrosion inhibition of carbon steel by 5-(chloromethyl)-8-quinolinol hydrochloride in hydrochloric acid solution. J Mol Liq 219:396–404
50. Khaled KF (2008) Molecular simulation, quantum chemical calculations and electrochemical studies for inhibition of mild steel by triazoles. Electrochim Acta 53:3484–3492
51. Devi PN, Sathiyabama J, Rajendran S (2017) Study of surface morphology and inhibition efficiency of mild steel in simulated concrete pore solution by lactic acid–Zn^{2+} system. Int J Corros Scale Inhib 6(1):18–31
52. Akalezi CO, Ogukwe CE, Ejele EA, Oguzie EE (2016) Corrosion inhibition properties of *Gongronema latifollium* extract in acidic media. Int J Corros Scale Inhib 5(3):232–247